A&A 518, L37 (2010)
DOI: 10.1051/0004-6361/201014558

Astronomy & Astrophysics
Special feature

Herschel: the first science highlights

Letter to the Editor

Probing the molecular interstellar medium of M82 with *Herschel*-SPIRE spectroscopy⋆

P. Panuzzo[1], N. Rangwala[2], A. Rykala[3], K. G. Isaak[3,4], J. Glenn[2], C. D. Wilson[5], R. Auld[3], M. Baes[6], M. J. Barlow[7], G. J. Bendo[8], J. J. Bock[9], A. Boselli[10], M. Bradford[9], V. Buat[10], N. Castro-Rodríguez[11], P. Chanial[1], S. Charlot[12], L. Ciesla[10], D. L. Clements[8], A. Cooray[13], D. Cormier[1], L. Cortese[3], J. I. Davies[3], E. Dwek[14], S. A. Eales[3], D. Elbaz[1], T. Fulton[15], M. Galametz[1], F. Galliano[1], W. K. Gear[3], H. L. Gomez[3], M. Griffin[3], S. Hony[1], L. R. Levenson[9], N. Lu[9], S. Madden[1], B. O'Halloran[8], K. Okumura[1], S. Oliver[16], M. J. Page[17], A. Papageorgiou[3], T. J. Parkin[5], I. Pérez-Fournon[11], M. Pohlen[3], E. T. Polehampton[18,19], E. E. Rigby[20], H. Roussel[12], N. Sacchi[21], M. Sauvage[1], B. Schulz[22], M. R. P. Schirm[5], M. W. L. Smith[3], L. Spinoglio[21], J. A. Stevens[23], S. Srinivasan[12], M. Symeonidis[17], B. Swinyard[18], M. Trichas[8], M. Vaccari[24], L. Vigroux[12], H. Wozniak[25], G. S. Wright[26], and W. W. Zeilinger[27]

(Affiliations are available in the online edition)

Received 30 March 2010 / Accepted 28 April 2010

ABSTRACT

We present the observations of the starburst galaxy M82 taken with the *Herschel* SPIRE Fourier-transform spectrometer. The spectrum (194–671 μm) shows a prominent CO rotational ladder from J = 4–3 to 13–12 emitted by the central region of M82. The fundamental properties of the gas are well constrained by the high J lines observed for the first time. Radiative transfer modeling of these high-S/N ^{12}CO and ^{13}CO lines strongly indicates a very warm molecular gas component at ~500 K and pressure of $\sim 3 \times 10^6$ K cm^{-3}, in good agreement with the H_2 rotational lines measurements from *Spitzer* and ISO. We suggest that this warm gas is heated by dissipation of turbulence in the interstellar medium (ISM) rather than X-rays or UV flux from the straburst. This paper illustrates the promise of the SPIRE FTS for the study of the ISM of nearby galaxies.

Key words. galaxies: ISM – galaxies: starburst – galaxies: individual: M82 – ISM: molecules – submillimeter: galaxies

1. Introduction

Starburst galaxies provide us with the opportunity to study star formation and its effect on the interstellar medium (ISM) in extreme environments. These galaxies combine large central gas concentrations and high ionizing radiation fields, resulting in bright molecular, neutral and ionized gas emission lines.

At a distance of 3.9 Mpc (Sakai & Madore 1999), M82 is the most well-studied starburst galaxy in the local universe, and it is widely used as a starburst prototype in cosmological studies. Its infrared luminosity (5.6×10^{10} $L_\odot$, Sanders et al. 2003) corresponds to a star-formation rate of 9.8 $M_\odot$ yr^{-1}, which has almost certainly been enhanced by its interaction with M81 and NGC 3077 (Yun et al. 1993). With a reported molecular gas content of 1.3×10^9 $M_\odot$ (Walter et al. 2002), its bright emission lines of CO and other molecules allow us to study its ISM in great detail (Shen & Lo 1995; Walter et al. 2002; Ward et al. 2003).

Far-infrared fine structure lines were used to constrain the physical properties of the ionized gas and photo-dissociation regions (PDRs) in M82. Colbert et al. (1999) found that the ionized gas emission can be reproduced with a 3–5 Myr old instantaneous starburst and a gas density of 250 cm^{-3}, while the PDR component is best fit with a density of 2000 cm^{-3}, in pressure equilibrium with the ionized phase.

Stellar evolution and photoionization models (Förster Schreiber et al. 2003) indicate a series of a few, Myr-duration starbursts with a peak of activity 10 Myr ago in the central regions, and 5 Myr ago in the circumnuclear ring. Models of the PDR and molecular emission as a set of non-interacting hot bubbles driving spherical shells of swept-up gas into a surrounding uniform medium also predict a starburst age of 5–10 Myr, but fail to match the observed far-infrared luminosity (Yao 2009).

The strengths of the CO lines place fundamental constraints on the physical properties of the molecular gas. Tilanus et al. (1991) fitted ^{12}CO and ^{13}CO lines from the central starburst up to J = 3–2 with a single-component model with temperatures of 30–55 K and densities of $3–7 \times 10^3$ cm^{-3}. Wild et al. (1992) used lines up to the CO J = 6–5 transition to refine these parameters to 40–50 K and ~10^4 cm^{-3}, while HCN and HCO$^+$ lines suggested densities greater than 3×10^5 cm^{-3} are present. Petitpas & Wilson (2000) showed evidence for a temperature or density gradient across the starburst region. Weiss et al. (2005) showed that CO emission up to J = 3–2 is dominated by more extended regions while higher J transitions originate in the central disk.

In this paper, we present observations of M82 with *Herschel* (Pilbratt et al. 2010) using the SPIRE Fourier-transform spectrometer (FTS) (Griffin et al. 2010), which measures the complete far-infrared spectrum from 194 to 671 μm. This spectral region is particularly interesting for probing the peak of the CO spectral line energy distribution (SLED) in gas-rich galaxies. The wealth of lines across a continuous spectral region allows

⋆ *Herschel* is an ESA space observatory with science instruments provided by European-led Principal Investigator consortia and with important participation from NASA.

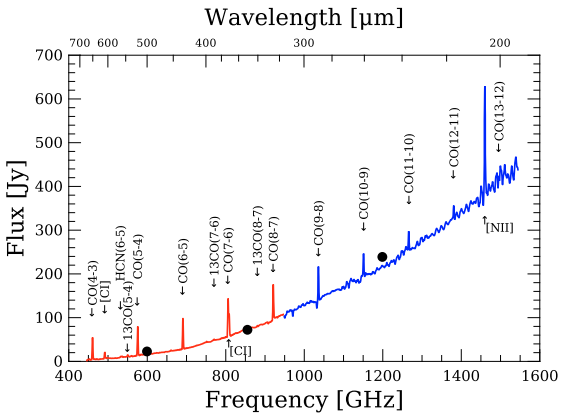

Fig. 1. Apodized spectrum of M82 corresponding to a 43.″4 beam, where red and blue lines represent data from the long- and the short-wavelength FTS bands respectively. Filled circles show SPIRE fluxes measured in the same beam.

for unprecedented precision in modeling the physical and chemical properties of the molecular ISM. Here, we focus on the measurement and analysis of the CO rotational transitions from the central starburst in M82.

2. Observations and data reduction

The galaxy M82 was observed by the SPIRE FTS in the high spectral resolution ($FWHM = 0.048$ cm^{-1}), point-source mode, on 2009 September 21 as a performance verification target. The total integration time was 1332 s. The data were processed and calibrated as described in Swinyard et al. (2010). Only data from the central detectors in the two FTS bands are presented here.

The beam size of the FTS bolometers varies with wavelength across the individual bands (see Swinyard et al. 2010), and the spatial extent of the M82 central starburst is comparable to the beam size (mean $FWHM \sim 19''$ and $35''$ for the short- and the long-wavelength bands respectively). For a proper comparison with models, the spectrum must be scaled appropriately to a single beam size by a source-beam coupling factor ($\eta_c(\nu)$). This factor was obtained by convolving the M82 SPIRE photometer map at 250 μm (Roussel et al. 2010), which has a beam $FWHM$ of 18.″1 (Griffin et al. 2010), with appropriate Gaussian profiles to reproduce the light distribution as seen by FTS bolometers at different beam sizes. The value of $\eta_c(\nu)$ is then given by the ratio of the beam-integrated flux density of the map convolved to the beam size corresponding to the given frequency (ν) to the beam-integrated flux density of the map with the largest beam size (43.″4); its values goes from 1 to 0.42. This implicitly assumes that the dust and CO emission distributions within the beam are the same at all frequencies.

We opted to use the extended-source calibrated[1] spectrum because the point-source calibration was more noisy and suffered from significant uncertainties below 600 GHz. We found, however, that the extended-source calibrated spectrum corrected for source-beam coupling is around a factor of 2 fainter than photometry for the same beam. We thus scaled the spectrum to match the photometry in the three bands by applying a single constant scaling factor for the short-wavelength band and a factor with a linear dependence on frequency for the long-wavelength band. The resulting spectrum is shown in Fig. 1 (for clarity, we show the spectrum apodized using the extended Norton-Beer function 1.5 from Naylor & Tahic 2007); we note that the short- and long-wavelength bands match very smoothly.

[1] Extended-source flux calibration is derived from telescope emission measurements, while the point-source flux calibration is based on observations of known astronomical point sources.

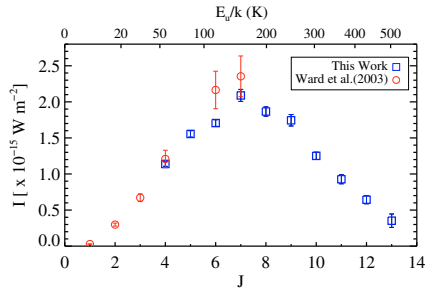

Fig. 2. ^{12}CO SLED for M82 for a 43.″4 beam as measured in this work (open squares) with 1σ statistical error bars. Ward et al. (2003) ground based data are shown by open circles.

Table 1. Measured fluxes of detected emission lines.

Transition name	Frequency (rest, GHz)	Flux (10^3 Jy km s^{-1})	Flux (10^{-16} W m^{-2})
^{12}CO J = 4–3	461.041	74.1 ± 2.2	11.32 ± 0.33
^{12}CO J = 5–4	576.268	80.9 ± 2.3	15.53 ± 0.45
^{12}CO J = 6–5	691.473	74.0 ± 2.0	17.04 ± 0.46
^{12}CO J = 7–6	806.652	77.7 ± 3.1	20.89 ± 0.84
^{12}CO J = 8–7	921.800	60.7 ± 2.1	18.64 ± 0.65
^{12}CO J = 9–8	1036.912	50.5 ± 2.3	17.44 ± 0.79
^{12}CO J = 10–9	1151.985	32.6 ± 1.3	12.51 ± 0.50
^{12}CO J = 11–10	1267.014	21.9 ± 1.5	9.28 ± 0.63
^{12}CO J = 12–11	1381.995	14.0 ± 1.2	6.44 ± 0.57
^{12}CO J = 13–12	1496.922	7.1 ± 1.9	3.53 ± 0.93
^{13}CO J = 5–4	550.926	5.3 ± 0.7	0.98 ± 0.12
^{13}CO J = 7–6	771.184	3.2 ± 0.6	0.81 ± 0.16
^{13}CO J = 8–7	881.273	2.3 ± 0.7	0.68 ± 0.22
HCN J = 6–5	531.716	2.9 ± 0.7	0.52 ± 0.12
[C I] $^3P_1 \rightarrow {}^3P_0$	492.161	20.6 ± 1.6	3.38 ± 0.26
[C I] $^3P_2 \rightarrow {}^3P_1$	809.342	43.2 ± 0.9	11.66 ± 0.25
[N II] $^3P_1 \rightarrow {}^3P_0$	1462.000	124.1 ± 5.8	60.51 ± 2.85

Notes. Errors are 1σ only from line fitting procedure, not including other uncertainties (see text). The ^{13}CO J = 6–5 line is missing due to fringing.

Line fluxes were recovered from the calibrated unapodized spectrum using a custom-written tool. It first subtracts the underlying continuum using a grey-body fit, then it removes any remaining large-scale ripples using a polynomial function. Emission lines were extracted by fitting sinc-convolved Gaussian line profiles. The strongest line is fitted first and then subtracted, with the process repeated until no line is found above a pre-set discrimination level. The integrated line fluxes were obtained by calculating the area under the fit. Table 1 lists the line fluxes and their 1σ uncertainties derived from the fitting procedure. In addition to the reported uncertainties we should include the following contributions: (i) the uncertainty in the estimation of the source-beam coupling factor due to the uncertainty in the beam profile and the assumption of identical distributions for dust and CO emission; and (ii) the uncertainty involved in the scaling the spectrum to match the photometric data, and in the measurement of photometric data. We conservatively suggest an uncertainty of ~30% for the line fluxes due to the above factors.

Figure 2 shows the ^{12}CO SLED, which peaks at the J = 7–6 line. In the same plot, we draw ground-based data compiled by Ward et al. (2003) (W03 hereafter). These data were measured with a smaller beam size, but were given for two observed lobes. In the plot we used the sum of the fluxes measured in the two lobes (which have a small overlap, but fit within the 43.″4 beam).

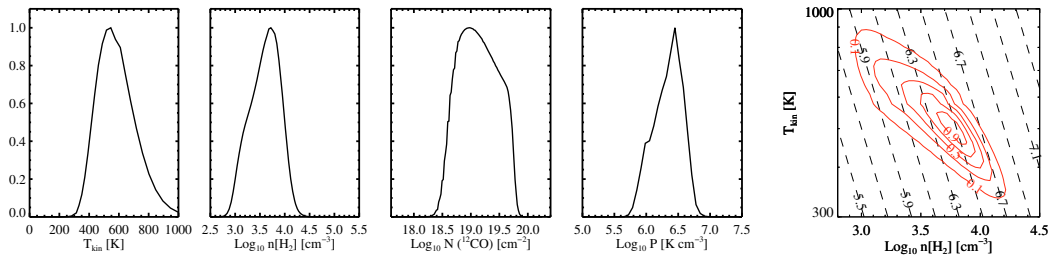

Fig. 3. *Left panel*: likelihood distributions of kinetic temperature, density, CO column density and pressure. *Right panel*: likelihood contour plot of temperature and density. Dashed lines show constant pressure ($\mathrm{Log}_{10}\ P\ (\mathrm{K\,cm^{-3}})$) relations.

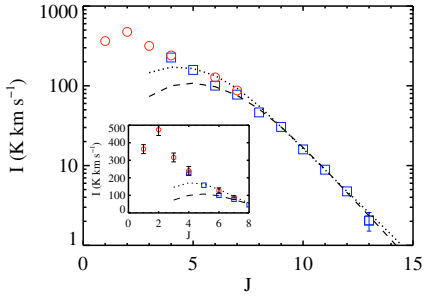

Fig. 4. Comparing the highest likelihood model (dotted line) with our CO line intensities. The model shown by a dashed line was obtained by using only J ≥ 7 – 6 CO lines. The W03 data are shown by open circles. The inset highlights the deviations from models at the lower J end.

3. Radiative transfer modeling

We used RADEX (van der Tak et al. 2007), a non-LTE code that computes the intensities of molecular lines by iteratively solving for statistical equilibrium using an escape-probability formalism assuming a uniform expanding sphere, to model the CO line intensities. The main inputs to RADEX are the gas density ($n_{\mathrm{H_2}}$), the kinetic temperature (T_{kin}), and the CO column density per unit line width ($N(^{12}\mathrm{CO})/\Delta\mathrm{v}$). We ran the code for a large parameter grid in T_{kin} (20–1000 K), $n_{\mathrm{H_2}}$ (10^2–10^6 cm^{-3}), $N(^{12}\mathrm{CO})$ (10^{15}–10^{18} cm^{-2}), and $N(^{13}\mathrm{CO})$ (10^{13}–10^{17}cm^{-2}). From this grid of models, we generated likelihood distributions by adapting the method described in W03, for T_{kin}, $n_{\mathrm{H_2}}$, $N(^{12}\mathrm{CO})$, $N(^{13}\mathrm{CO})$, and pressure by comparing the RADEX and observed line fluxes.

To avoid any non-physical situation we applied two priors in this analysis following W03. The first one limits the ^{12}CO column density in a way that the total mass of the molecular gas producing the CO lines cannot exceed the dynamical mass of the galaxy according to the following relation:

$$N(^{12}\mathrm{CO}) < \frac{M_{\mathrm{dyn}} x_{\mathrm{CO}}}{\mu m_{\mathrm{H_2}}} \frac{1}{\pi R_{\mathrm{d}}^2} = 2.3 \times 10^{20}\ \mathrm{cm^{-2}}\ , \qquad (1)$$

where the dynamical mass of the disk $M_{\mathrm{dyn}} = 2.4 \times 10^9\ M_\odot$, the radius of the disk $R_{\mathrm{d}} = 250$ pc, the abundance of CO relative to H_2, $x_{\mathrm{CO}} = 3 \times 10^{-4}$ (W03), and $\mu = 1.4$ is the mean molecular weight in units of $m_{\mathrm{H_2}}$. The second prior limits the column length to be less than that of the entire molecular region according to $\frac{N(\mathrm{CO})}{n(\mathrm{H_2}) x_{\mathrm{CO}}} < 1.54 \times 10^{21}$ cm. In this analysis we used all the ^{12}CO and ^{13}CO lines in Table 1 along with their 1σ statistical errors. It was necessary to add 20% and 10% uncertainties for the CO $J \leq$ 8–7 and $J >$ 8–7 lines, respectively, to avoid un-physically narrow and noisy distributions (consistent with the additional 30% line flux uncertainty estimate in Sect. 2). The resulting distributions are shown in Fig. 3 for each variable, marginalizing over the other variables. The modeling only depends on the relative line fluxes, therefore the results will not be affected by the uncertainties in the absolute flux calibration.

4. Results and discussion

We found that the highest likelihood model (dotted line in Fig. 4) provides a good fit to our data (open squares), in particular for the higher J lines ($J \geq$ 7–6). The likelihood contour plot of temperature and density in Fig. 3 (last panel) strongly indicates that the observed emission is coming from very warm gas with a kinetic temperature of ∼540 K and a pressure of $\sim 3 \times 10^6$ K cm^{-3}. The detailed physical characteristics of the warm gas are listed in Table 2, which are obtained from the likelihood distributions shown in Fig. 3.

The ISM of this galaxy has been well-studied using ground-based observations – in particular the lowest-lying CO rotational lines that provide constraints on the physical state of the cold molecular gas. Several studies from ground-based CO observations, including W03, have identified cold gas at ∼30 K. We show W03 data (open circles) over-plotted in Fig. 4. From $J \leq$ 7–6 lines, W03 deduced the presence of a warm component, in agreement with our finding, but with different temperature, mass and density. Having observations up to J = 13–12 enables a much better constraint to be placed on these parameters than is possible from the lower J lines. A colder gas component is also consistent with the deviation of our lower J lines, especially CO J = 4–3, from our highest-likelihood model. If we use only the higher-J lines ($J \geq$ 7–6) in our likelihood analysis, we get a model in better agreement with these lines while underpredicting the lower-J lines, supporting the hypothesis of a contribution of the colder component to those lines.

Assuming x_{CO} of 3×10^{-4} and an intrinsic line width of 180 km s^{-1} (W03), and using our beam-averaged CO column density we find the mass of warm gas to be $1.2 \times 10^7\ M_\odot$ within a beam area of about 2140 square arcseconds, likely covering most of the molecular emission from the galaxy. Using the mass of the cold gas from W03 we find a ratio of cold gas to the SPIRE-observed warm gas mass of ∼3. The best-fitting model predicts the optical depth for the CO lines, which peaks at a value of 1.7 for J = 6–5, and then drops to approximately 10^{-2} for J = 13–12.

Mid-IR H_2 rotational lines are optically-thin and easily thermalized, so they provide an independent constraint on the mass of warm gas. Several transitions have been studied with ISO (Rigopoulou et al. 2002) and *Spitzer* (Beirão et al. 2008). Both studies agree that the S(1) to S(2) line ratio suggests $T \sim 500$ K (assuming an ortho-to-para ratio of 3), in excellent agreement with our temperature. Using the *Spitzer* measurement of S(1) line flux corrected for our larger beam we calculate a mass of $\sim 2 \times 10^6\ M_\odot$. Given the uncertainty on x_{CO}, and considerable extinction ($\tau_{\mathrm{dust}} \gtrsim 1.5$; from dust models of Laor & Draine (1993) extrapolated to our wavelengths) of the S(1) line, we find it to be consistent with our mass range.

Our inferred thermal pressure (3×10^6 K cm^{-3}) is comparable to both that of the M 82 atomic gas as probed by the C II and O I transitions (Kaufman et al. 1999; Lord et al. 1995), and

Table 2. Model results and their uncertainties for the warm gas.

Quantity	Most probable value	Range[†]
$T_{\rm kin}$ (K)	545	350–825
$\mathrm{Log}_{10}\, n(\mathrm{H_2})$ ($\mathrm{cm^{-3}}$)	3.7	3.0–4.1
$\mathrm{Log}_{10} N(^{12}\mathrm{CO})$ ($\mathrm{cm^{-2}}$)	19.0	18.5–19.8
$\mathrm{Log}_{10}\, \Phi_A N(^{12}\mathrm{CO})^{\dagger}$ ($\mathrm{cm^{-2}}$)	17.4	17.2 – 17.9
$N(^{12}\mathrm{CO})/N(^{13}\mathrm{CO})$	20	15 – 37
$\mathrm{Log}_{10} P$ (K $\mathrm{cm^{-3}}$)	6.4	5.8–6.7
$M_{\rm gas}$ ($\times 10^7\ M_\odot$)	1.2	0.7–3.6

Notes. [(†)] Ranges are for 95% confidence intervals; [(††)] Beam averaged column density where $\Phi_{\rm A}$ is an area filling factor.

the UV-shielded dense gas (Naylor et al. 2010), although this does not imply pressure equilibrium between the phases. Our warm-component mass is also similar to the $9 \times 10^6\ M_\odot$ inferred from the photodissociation region (PDR) analysis based on the atomic gas lines (Kaufman et al. 1999). However, the CO emission in the warm molecular gas likely does not arise from PDRs. This is because we measure CO transitions that are much more luminous than predicted by the PDR models. These models require an extremely high density PDR ($n > 10^5$) to reproduce the J = 6–5 and 7–6 intensities, a condition which is clearly ruled out by the atomic lines and their ratio to the far-IR flux.

At a temperature of about 500 K, H_2 will be the dominant coolant compared to CO. This is evident from the observed H_2 line luminosities, and agrees with the model predictions (Neufeld et al. 1995; Le Bourlot et al. 1998). The models predict H_2 cooling of $\sim 10^{-22.6}$ ergs $\mathrm{s^{-1}}$ per molecule for the temperature and density of SPIRE-observed warm gas. This implies a total molecular gas cooling of about 2.6 $L_\odot/M_\odot$; i.e., $1.2 \times 10^7\ M_\odot$ of gas will radiate about $3 \times 10^7\ L_\odot$ in H_2 lines, in good agreement with the value derived from ISO and *Spitzer* data.

What is the heating source of this warm molecular gas? Hard X-rays from an AGN have the potential for heating molecular gas in an XDR (Maloney et al. 1996), but there is no strong evidence for an AGN in M82 (Strickland & Heckman 2007). Moreover, with a strong XDR component, such as seen in Mrk231 (van der Werf et al. 2010), the SLED becomes flat at high J instead of decreasing as in M82. Another scenario is heating via the enhanced cosmic ray density generated by the high supernova rate in the nuclear starburst (Suchkov et al. 1993). With a cosmic ray energy deposition rate of 3.5–12×10^{-16} eV $\mathrm{s^{-1}}$ per H_2 molecule in the Galaxy (Goldsmith & Langer 1978; van Dishoeck, & Black 1986), the energy input per mass in M82 is 0.09 to 0.3 $L_\odot/M_\odot$, too low to match the observed cooling.

A second possibility is heating from the dissipation of turbulence (Falgarone & Puget 1995; Mac Low 1999; Pan & Padoan 2009). Using a velocity gradient of 35 km $\mathrm{s^{-1}}$ $\mathrm{pc^{-1}}$ computed from our best fit RADEX model and a typical sizescale (or Jeans length) between 0.3 to 1.6 pc in the expression for turbulent heating per unit mass from Bradford et al. (2005), we can match the observed cooling of 2.6 $L_\odot/M_\odot$. Our velocity gradient is large, particularly when compared with the few km $\mathrm{s^{-1}}$ velocity spread found on 1 pc scales in Galactic star-forming sites, but may not be unreasonable in M82 given the powerful stellar winds known to be present in the starburst.

5. Conclusions

We have presented the *Herschel*-SPIRE spectroscopic observations of the starburst galaxy M82. The spectra show a prominent CO emission-line ladder along with C I and N II lines. Radiative transfer modeling of CO lines clearly indicates a warm gas component at ~500 K in addition to the cold (~30 K) component derived from ground-based studies. The properties of the warm gas are strongly constrained by the high J lines, observed here for the first time. The temperature and mass of warm gas agree with the H_2 rotational lines observations from *Spitzer* and ISO. At this temperature H_2 is the dominant coolant instead of CO, and we argue that turbulence from stellar winds and supernovae may be the dominant heating mechanism.

Acknowledgements. We are grateful to P. Maloney for his advices on radiative transfer modeling, and to the SPIRE FTS team for assistance with data reduction. SPIRE has been developed by a consortium of institutes led by Cardiff University (UK) and including Univ. Lethbridge (Canada); NAOC (China); CEA, OAMP (France); IFSI, Univ. Padua (Italy); IAC (Spain); Stockholm Observatory (Sweden); Imperial College London, RAL, UCL-MSSL, UKATC, Univ. Sussex (UK); and Caltech/JPL, IPAC, Univ. Colorado (USA). This development has been supported by national funding agencies: CSA (Canada); NAOC (China); CEA, CNES, CNRS (France); ASI (Italy); MCINN (Spain); SNSB (Sweden); STFC (UK); and NASA (USA). Additional funding support for some instrument activities has been provided by ESA.

References

Beirão, P., Brandl, B. R., Appleton, P. N., et al. 2008, ApJ, 676, 304
Bradford, C. M., Stacey, G. J., Nikola, T., et al. 2005, ApJ, 623, 866
Colbert, J. W., Malkan, M. A., Clegg, P. E., et al. 1999, ApJ, 511, 721
Falgarone, E., & Puget, J.-L. 1995, A&A, 293, 840
Förster Schreiber, N. M., Genzel, R., Lutz, D., et al. 2003, ApJ, 599, 193
Goldsmith, P. F., & Langer, W. D. 1978, ApJ, 222, 881
Griffin, M. J., et al. 2010, A&A, 518, L3
Kaufman, M. J., Wolfire, M. G., Hollenbach, D. J., & Luhman, M. L. 1999, ApJ, 527, 795
Kaufman, M. J., Wolfire, M. G., & Hollenbach, D. J. 2006, ApJ, 644, 283
Mac Low, M.-M. 1999, ApJ, 524, 169
Maloney, P. R., Hollenbach, D. J., & Tielens, A. G. G. M. 1996, ApJ, 466, 561
Naylor, B. J., Bradford, C. M., Aguirre, J. E., et al. 2010, ApJ, submitted
Naylor, D. A., & Tahic M. K. 2007, J. Opt. Soc. Am. A, 24, 3644
Neufeld, D. A., Lepp, S., & Melnick, G. J. 1995, ApJS, 100, 132
Laor, A., & Draine, B. T. 1993, ApJ, 402, 441
Le Bourlot, J., Pineau des Forêts, G., & Flower, D. R. 1999, MNRAS, 305, 802
Lord, S. D., Hollenbach, D. J., Colgan, S. W. J., et al. 1995, ASPC, 73, 151
Pan, L., & Padoan, P. 2009, ApJ, 692, 594
Petitpas, G. R., & Wilson, C. D. 2000, ApJ, 538, L117
Pilbratt, G. L., et al. 2010, A&A, 518, L1
Rigopoulou, D., Kunze, D., Lutz, D., Genzel, R., & Moorwood, A. F. M. 2002, A&A, 389, 374
Roussel, H., et al. 2010, A&A, 518, L66
Sakai, S., & Madore, B. F. 1999, ApJ, 526, 599
Sanders, D. B., Mazzarella, J. M., Kim, D.-C., Surace, J. A., & Soifer, B. T. 2003, AJ, 126, 1607
Seaquist, E. R., Lee, S. W., & Moriarty-Schieven, G. H. 2006, ApJ, 638, 148
Shen, J., & Lo, K. Y. 1995, ApJ, 445, L99
Strickland, D. K., & Heckman, T. M. 2007, ApJ, 658, 258
Suchkov, A., Allen, R. J., & Heckman, T. M. 1993, ApJ, 413, 542
Swinyard, B. G., et al. 2010, A&A, 518, L4
Tilanus, R. P. J., Tacconi, L. J., Sutton, E. C., et al. 1991, ApJ, 376, 500
van der Tak, F. F. S., Black, J. H., Schöier, F. L., A&A, 468, 627
van der Werf, P. P., et al. 2010, A&A, 518, L42
van Dishoeck, E. F., & Black, J. H. 1986, ApJS, 62, 109
Walter, F., Weiss, A., & Scoville, N. 2002, ApJ, 580, L21
Ward, J. S., Zmuidzinas, J., Harris, A. I., et al. 2003, ApJ, 587, 171 (W03)
Weiss, A., Walter, F., & Scoville, N. Z. 2005, A&A, 438, 533
Wild, W., Harris, A. I., Eckart, A., et al. 1992, A&A, 265, 447
Yao, L. 2009, ApJ, 705, 766
Yun, M. S., Ho, P. T. P., & Lo, K. Y. 1993, ApJ, 411, L17

[1] CEA, Laboratoire AIM, Irfu/SAp, Orme des Merisiers, 91191 Gif-sur-Yvette, France
e-mail: pasquale.panuzzo@cea.fr
[2] Dept. of Astrophysical & Planetary Sciences, CASA CB-389, University of Colorado, Boulder, CO 80309, USA
[3] School of Physics & Astronomy, Cardiff University, Queens Buildings The Parade, Cardiff CF24 3AA, UK
[4] ESA Astrophysics Missions Division, ESTEC, PO Box 299, 2200 AG Noordwijk, The Netherlands
[5] Dept. of Physics & Astronomy, McMaster University, Hamilton, Ontario, L8S 4M1, Canada
[6] Sterrenkundig Observatorium, Universiteit Gent, Krijgslaan 281 S9, 9000 Gent, Belgium
[7] Dept. of Physics & Astronomy, University College London, Gower Street, London WC1E 6BT, UK
[8] Astrophysics Group, Imperial College, Blackett Laboratory, Prince Consort Road, London SW7 2AZ, UK
[9] JPL, Pasadena, CA 91109, United States; Dept. of Astronomy, California Institute of Technology, Pasadena, CA 91125, USA
[10] Laboratoire d'Astrophysique de Marseille, UMR6110 CNRS, 38 rue F. Joliot-Curie, 13388 Marseille, France
[11] Instituto de Astrofísica de Canarias (IAC) and Departamento de Astrofísica, Universidad de La Laguna (ULL), La Laguna, Tenerife, Spain
[12] Institut d'Astrophysique de Paris, UMR7095 CNRS, Université Pierre & Marie Curie, 98 bis Boulevard Arago, 75014 Paris, France
[13] Dept. of Physics & Astronomy, University of California, Irvine, CA 92697, USA
[14] Observational Cosmology Lab, Code 665, NASA Goddard Space Flight Center Greenbelt, MD 20771, USA
[15] Blue Sky Spectroscopy, Alberta, T1J 1B1, Canada
[16] Dept. of Physics and Astronomy, University of Sussex, Brighton, BN1 9QH, UK
[17] Mullard Space Science Laboratory, University College London, Holmbury St Mary, Dorking, Surrey RH5 6NT, UK
[18] Space Science and Technology Department, Rutherford Appleton Laboratory, Oxfordshire, OX11 0QX, UK
[19] Institute for Space Imaging Science, University of Lethbridge, Lethbridge, Alberta, T1K 3M4, Canada
[20] School of Physics & Astronomy, University of Nottingham, University Park, Nottingham NG7 2RD, UK
[21] Istituto di Fisica dello Spazio Interplanetario, INAF, Via del Fosso del Cavaliere 100, 00133 Roma, Italy
[22] IPAC, California Institute of Technology, Mail Code 100-22, 770 South Wilson Av, Pasadena, CA 91125, USA
[23] Centre for Astrophysics Research, Science & Technology Research Centre, University of Hertfordshire, College Lane, Herts AL10 9AB, UK
[24] University of Padova, Dept. of Astronomy, Vicolo Osservatorio 3, 35122 Padova, Italy
[25] Observatoire Astronomique de Strasbourg, UMR 7550 Université de Strasbourg - CNRS, 11, rue de l'Université, 67000 Strasbourg, France
[26] UK Astronomy Technology Center, Royal Observatory Edinburgh, Edinburgh, EH9 3HJ, UK
[27] Institut für Astronomie, Universität Wien, Türkenschanzstr. 17, 1180 Wien, Austria